J. Fluid Mech. (2014), *vol.* 746, *pp.* 5–30. © Cambridge University Press 2014
doi:10.1017/jfm.2014.103

On the self-similar exact MHD jet solution

R. I. Mullyadzhanov and N. I. Yavorsky†

Institute of Thermophysics SB RAS, Lavrentyeva str. 1, Novosibirsk 630090, Russia
Novosibirsk State University, Pirogova str. 2, Novosibirsk, 630090, Russia

(Received 22 August 2011; revised 5 November 2013; accepted 20 February 2014;
first published online 28 March 2014)

We consider an axisymmetric steady flow of a viscous incompressible conducting fluid. The flow is induced by the point source of momentum and point electrode discharging the electric current, both of which are located at the end of a thin semi-infinite insulated wire. We seek the solution in the conical self-similar class where the velocity and magnetic field decrease as the inverse distance from the origin. The solution is obtained for various parameters of the problem, namely the Reynolds number, dimensionless electric current and Batchelor number (magnetic Prandtl number). A reverse flow along the wire occurs, leading to the confinement of the current density in the direction of the jet. If the Batchelor number is zero, the solution obtains a singularity at finite values of the current leading to its breakdown; otherwise, the solution exists at all parameter values. We derive the boundary-layer equations near the wire for large current values and obtain the solution. The pitchfork bifurcation with non-zero poloidal magnetic field occurs and causes the rotation of the fluid, which eliminates the current confinement effect. We describe the conditions when the solution for the swirling jet exists. The connection of this problem to the ones considered previously is discussed.

Key words: jets, magneto convection, nonlinear instability, vortex dynamics

1. Introduction

In some industrial processes (e.g. electric arc welding, electroslag welding) as well as natural phenomena (lightning discharge, tornado, astrophysical jets) moving media represented by the conducting fluid model include a magnetic field that is likely to change the nature of the motion. The electric current and magnetic field determine the Lorentz force acting on a moving medium. Due to the nonlinear interaction of the mechanical motion and the magnetic field, physical effects caused by the formation of positive feedbacks in the MHD system are accompanied by the bifurcations of new types of motion.

The case when the radial current is produced by a point electrode located on the surface of the half-space is a simple model of some metallurgical processes. It belongs to the class of exact solutions of the Navier–Stokes equations. The first solutions of this type were obtained by Slezkin (1934), Landau (1944) and Squire (1951) for infinite space and Squire (1952) for the half-space, which correspond to

† Email address for correspondence: nick@itp.nsc.ru

https://doi.org/10.1017/jfm.2014.103 Published online by Cambridge University Press

an axisymmetric submerged jet of a viscous incompressible non-conducting fluid induced by a point force. Since these problems do not include a natural length scale, the solution is self-similar corresponding to conical flows, where the velocity is inversely proportional to the distance from the origin. Wu (1961) was the first to consider the solution of the MHD equations in the conical class. He studied the flow of the conducting fluid with non-zero poloidal components of the velocity and magnetic field. Following Landau (1944) and Squire (1952), Wu obtained a system of ordinary differential equations for the velocity and magnetic field and analysed components of the momentum flux tensor. Then he provided two solutions for the flow in infinite space and half-space with the expansion of all functions of the problem in a series of $Bt = \nu/\lambda \ll 1$, where ν is the kinematic viscosity of the fluid, $\lambda = (\mu\sigma)^{-1}$ is the magnetic diffusivity, μ is the magnetic permeability and σ is the conductivity of the medium. The general problem of the flow of a conducting fluid, with all components of the velocity and magnetic field decreasing as the inverse distance from the origin, was formulated by Shcherbinin (1969).

It is known that in conical flows the solutions may lose existence (the so-called collapse) at finite parameter values of the problem. Goldshtik (1960) was the first to find this self-similar solution. A semi-infinite vortex line with a given circulation hitting the wall at the right angle generates a flow in the half-space; at the same time the velocity on the axis tends to infinity as the circulation tends to its critical value. Serrin (1972) generalized the problem of the vortex line by allowing a logarithmic singularity of the angle function of the radial velocity at the axis, which involved a new free parameter, namely the coefficient of the logarithm corresponding to the magnitude of the force acting along the symmetry axis. In this case, the solution existed at all values of the Reynolds number determined by the circulation of the vortex line. Serrin found that the structure of the flow had either one or two cells. Yih *et al.* (1982) considered a flow field induced by the rotating cone wall.

The meridional flow produced by the vortex line (Goldshtik 1960) is similar to the flow in the half-space induced by the Lorentz force when the electric current is discharged from a point electrode placed on the surface. Several assumptions can be used to simplify the analysis. The approximation $Bt \ll 1$ is frequently employed in liquid metal MHD due to the specific properties of the materials studied. In this case, the flow does not affect the distribution of the magnetic field, while the radial current from the point electrode is isotropic. Based on this assumption, Lundquist (1969) obtained a solution for a creeping flow of a viscous fluid by studying a linear problem neglecting convective terms. Shercliff (1970) studied this problem for an ideal fluid and found a solution with the velocity singularity on the symmetry axis. Later Sozou (1971) considered the problem for the full Navier–Stokes equations and showed that when the dimensionless parameter $S = \mu I^2(4\pi^2\rho\nu^2)^{-1}$, where I is the total current discharged from the point electrode, ρ is the fluid density, reaches the critical value $S = S_c = 150$, the velocity has a singularity on the axis of symmetry (collapse). This effect is similar to that described by Goldshtik (1960). Narain & Uberoi (1971) and Narain & Uberoi (1973) studied Sozou's problem, changing θ_0, which was the angle between the axis of symmetry and the cone wall, with the point electrode placed at the vertex of the cone. Thus, they showed that as θ_0 decreased S_c increased. Sozou (1972) and Tsinober (1973) used various approaches to study a non-self-similar problem of the flow of a conducting fluid with a point electrode and source of fluid of a given flow rate located at the origin. Sozou & English (1972) considered the influence of the fluid flow on the current distribution by studying finite Bt. They estimated the existence region of the solution in the space of (S, Bt) parameters and showed that the critical value S_c increased with the increase in Bt.

https://doi.org/10.1017/jfm.2014.103 Published online by Cambridge University Press

In this paper we study the case of $\theta_0 = \pi$; thus, a point electrode is located at the end of a semi-infinite immersed insulated wire. Note that the no-slip condition on the wire cannot be satisfied in the class of self-similar solutions for conical flows. A similar case was investigated by Shcherbinin (1973), who considered two flow regions of non-conducting and conducting fluid (gas discharge model). However, in order to satisfy the no-slip condition on the wire, Shcherbinin neglected the pressure continuity condition at the boundary between these two regions. The problem of the infinitely thin wire with a point electrode at the end interacting with a normal rigid plane or a free surface was solved by Bojarevics (1981); the equations for this problem allow the no-slip condition on the wire since the problem is formulated in the half-space. Similar and other problems were generalized and presented in works by Bojarevics *et al.* (1989), Moreau (1990), Davidson (2001) and Shtern (2012).

As Wu (1961) extended the class of exact solutions for conical flows to MHD, Pao & Long (1966) summarized the works of Long (1958) and Long (1961), which consider a vortex line in infinite space in the boundary-layer approximation. Pao & Long (1966) studied a Long's jet vortex which is due to a source of linear momentum and angular momentum and also due to a source of electric current and magnetic field.

There are solutions of the Navier–Stokes equations for swirling jets that are not based on a vortex line model. For instance, swirling jets may occur as a result of the steady bifurcation at certain parameters from an axisymmetric flow, which is supported by numerous examples of solutions for conical flows. Steady bifurcations were studied by Shtern & Barrero (1995); Shtern & Hussain (1998) regarded certain approaches to the stability problem in conical flows; striking features of conical flows such as collapse and bifurcations were discussed by Shtern & Hussain (1999). Steady bifurcations are also considered in MHD problems. Goldshtik & Shtern (1989) expanded the problem of the interaction of a vortex line with a plane to the flow of a conducting fluid, with a given velocity on the axis of symmetry. They showed that the magnetic field could be self-excited at certain parameters. Bojarevics, Millere & Chaikovsky (1981) observed how mercury started to rotate around the symmetry axis in a semi-spherical container when the current was supplied to the free-surface of the fluid through an electrode. Bojarevics & Shcherbinin (1983) provided a self-similar solution of this problem for a swirling flow and discussed the mechanisms sustaining the rotation. Petrunin & Shtern (1993) found a steady bifurcation for Sozou's problem if $Bt \neq 0$, which caused self-excitation of the poloidal magnetic field along with the rotation of the fluid. However, Davidson *et al.* (1999) rightly stated that in order to explain the above experiment, a confined flow had to be taken into account since Ekman pumping was important. Furthermore, a reverse flow induced by the boundaries of the region determined the swirl generation. Davidson *et al.* (1999) investigated the distributed magnetic field instead of a point current source and suggested an explanation in terms of the suppression of the poloidal motion. Hence, the azimuthal force constituting a small share of the poloidal one (several per cent), generates the swirl, which in turn suppresses the meridional flow. These theoretical assumptions were later supported by Grants *et al.* (2008). Nevertheless, if the boundary effects are negligible, at certain parameters of the flow an azimuthal driving force appears which is strong enough to cause a swirling flow (Shtern & Barrero 1995). The steady bifurcation discussed in this paper is related to various examples of symmetry breaking in axisymmetric flows. Apparently, the general feature causing these phenomena is a convergent meridional flow.

In this paper, we study a flow induced by a point source of momentum and current which are both located at the end of a semi-infinite wire. This formulation provides

https://doi.org/10.1017/jfm.2014.103 Published online by Cambridge University Press

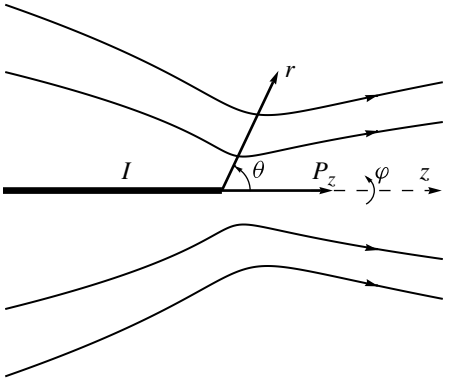


FIGURE 1. Problem scheme and coordinate system.

a model of the flow in a pool of conducting fluid with an immersed pipe of small diameter compared with the size of the pool. The conducting fluid with the electric current flows from this pipe. Since the wire (the pipe) is infinitely thin and not represented by a narrow cone, the radial velocity has a logarithmic singularity on the wire. However, due to this formulation, the values of the current and velocity on the symmetry axis are set independently. In this case, the current does not determine the mechanical momentum at the origin unlike the problem when the no-slip condition is satisfied on the wall of the cone (see § 7). This problem reveals different features of the solutions such as collapse discussed above, when the velocity singularity occurs in the flow field, and a bifurcation leading to the rotation of the fluid.

2. Problem formulation

The focus of the study is an axisymmetric MHD flow of a viscous incompressible conducting fluid in infinite space, generated by a point source of momentum P_z and point electrode discharging the electric current I, which are both located at the end of a semi-infinite insulated wire (figure 1). Physical parameters of the problem are considered to be constant.

The problem is described by the MHD equations (see Davidson 2001):

$$\frac{\mathrm{d}\boldsymbol{u}}{\mathrm{d}t} = -\frac{1}{\rho}\nabla p + \nu\nabla^2\boldsymbol{u} + \frac{1}{\mu\rho}(\nabla\times\boldsymbol{B})\times\boldsymbol{B}, \quad \nabla\cdot\boldsymbol{u} = 0, \tag{2.1}$$

$$\frac{\partial\boldsymbol{B}}{\partial t} = \nabla\times(\boldsymbol{u}\times\boldsymbol{B}) + \lambda\nabla^2\boldsymbol{B}, \quad \nabla\cdot\boldsymbol{B} = 0, \tag{2.2}$$

where $\boldsymbol{u}$ is the velocity vector and $\boldsymbol{B}$ is the magnetic field, p and ρ are the fluid pressure and density and $\mathrm{d}/\mathrm{d}t = \partial/\partial t + \boldsymbol{u}\cdot\nabla$ denotes the material derivative.

Let the origin of the spherical coordinate system (r, θ, φ) coincide with the source of momentum and current. This point and the area occupied by the wire do not belong to the flow region, where (2.1) and (2.2) are valid. In case of steady motion, in Cartesian coordinates they take the form (Landau & Lifshitz 1987)

$$\frac{\partial\Pi_{ij}}{\partial x_j} = 0, \quad \frac{\partial u_j}{\partial x_j} = 0, \quad \frac{\partial\Lambda_{ij}}{\partial x_j} = 0, \quad \frac{\partial B_j}{\partial x_j} = 0, \tag{2.3}$$

https://doi.org/10.1017/jfm.2014.103 Published online by Cambridge University Press

where Π_{ij} is the symmetric tensor of the total momentum flux and Λ_{ij} is the antisymmetric tensor defined as

$$\Pi_{ij} = \rho u_i u_j + \left(p + \frac{\boldsymbol{B}^2}{2\mu}\right)\delta_{ij} - \rho\nu\left(\frac{\partial u_i}{\partial x_j} + \frac{\partial u_j}{\partial x_i}\right) - \frac{B_i B_j}{\mu},$$
$$\Lambda_{ij} = B_i u_j - u_i B_j - \lambda\left(\frac{\partial B_i}{\partial x_j} - \frac{\partial B_j}{\partial x_i}\right), \tag{2.4}$$

and δ_{ij} is the Kronecker delta.

The problem formulation does not include a natural length scale. Thus, according to the dimensional analysis (Wu 1961) of MHD equations, we search for the solution of (2.3) as follows:

$$u_r = -\frac{\nu y'(x)}{r}, \quad u_\theta = -\frac{\nu y(x)}{r\sqrt{1-x^2}}, \quad u_\varphi = \frac{\nu\Gamma(x)}{r\sqrt{1-x^2}},$$
$$B_r = -\frac{\nu\sqrt{\rho\mu}\Phi'(x)}{r}, \quad B_\theta = -\frac{\nu\sqrt{\rho\mu}\Phi(x)}{r\sqrt{1-x^2}}, \quad B_\varphi = \frac{\nu\sqrt{\rho\mu}L(x)}{r\sqrt{1-x^2}}, \tag{2.5}$$
$$p = p_\infty + \frac{\rho\nu^2}{r^2}P(x),$$

where $x = \cos\theta$, prime denotes differentiation with respect to x, p_∞ is the pressure at $r \to \infty$. The solenoidal condition for the velocity and magnetic fields is satisfied automatically assuming the solution in the class (2.5). Substituting (2.5) into (2.3) (see appendix A), the system of ordinary differential equations is obtained:

$$(1-x^2)y' + 2xy - y^2/2 = F - \Phi^2/2, \tag{2.6}$$
$$(1-x^2)\Gamma'' = y\Gamma' - \Phi L', \tag{2.7}$$
$$(1-x^2)\Phi'' = Bt(y\Phi' - y'\Phi), \tag{2.8}$$
$$(1-x^2)L'' = Bt(yL' - \Phi\Gamma' + 2(y'L - \Phi'\Gamma) + 2x(yL - \Phi\Gamma)/(1-x^2)), \tag{2.9}$$
$$(1-x^2)F''' = 2\Gamma\Gamma' - 2LL'. \tag{2.10}$$

This system of equations is derived, for instance, by Goldshtik & Shtern (1989) in a slightly different form, where the last terms on the right-hand sides of (2.6), (2.7) and (2.10) have a dimensionless factor S, introduced in § 1. An auxiliary function F appears in the course of transformations to ease the analysis following Goldshtik (1960). The dimensionless criterion $Bt = \nu/\lambda$ (Batchelor number or magnetic Prandtl number), being a ratio of the kinematic viscosity to the magnetic diffusivity, characterizes the properties of the medium.

The dimensionless functions y, L, F, Γ and Φ are analytic in the entire flow region, except for the semi-axis $\theta = \pi$ ($x = -1$) occupied by the wire. We study their behaviour in the vicinity of this point in § 3. The jet flow is determined if two dimensionless parameters are set. We define the Reynolds number Re, based on the velocity on the semi-axis $x = 1$, and dimensionless current J

$$Re = \left.\frac{u_r r}{\nu}\right|_{x=1} = -y'(1), \quad J = \frac{I\sqrt{\mu/\rho}}{2\pi\nu}. \tag{2.11}$$

The radial velocity is finite and the jet profile is symmetric on the semi-axis $x = 1$, i.e.

$$|u_r| < \infty, \quad \frac{\partial u_r}{\partial\theta} = 0, \quad \theta = 0,$$

https://doi.org/10.1017/jfm.2014.103 Published online by Cambridge University Press

and in terms of y we obtain that

$$|y'(1)| < \infty, \quad \lim_{x\to 1}\left(\sqrt{1-x^2}y''\right) = 0, \tag{2.12}$$

which corresponds to y being analytic at $x=1$. If u_θ, u_ϕ and B_θ are bounded at $x=\pm 1$ while B_ϕ is bounded at $x=1$, due to (2.5) we get

$$y(\pm 1) = 0, \quad \Gamma(\pm 1) = 0, \quad \Phi(\pm 1) = 0, \quad L(1) = 0. \tag{2.13}$$

Using (2.5) and Ampere's law, we determine the current density

$$\boldsymbol{j} = \mu^{-1}\nabla \times \boldsymbol{B} = -r^{-2}\nu\sqrt{\rho\mu^{-1}}\left(L'\boldsymbol{e}_r + \sqrt{1-x^2}\Phi''\boldsymbol{e}_\varphi\right), \tag{2.14}$$

where $\boldsymbol{e}_r$ and $\boldsymbol{e}_\varphi$ are the spherical local orthogonal unit vectors. If we study the continuity equation signifying conservation of electrical charge, we can write

$$\oint j_r \mathrm{d}S = 2\pi \int_0^\pi j_r r^2 \sin\theta \,\mathrm{d}\theta = 2\pi\nu\sqrt{\rho\mu^{-1}}(L(-1) - L(1)) = I.$$

Hence, as long as $L(1) = 0$ we obtain $L(-1) = J$. Then according to (2.6) and conditions (2.13), $F(\pm 1) = 0$. Next, if we differentiate (2.6), we obtain that $F'(1) = 0$ with the use of (2.12) and (2.13). Let us integrate (2.10) and, since the integration constant is zero due to the boundary conditions and to the fact that F is analytic at $x=1$, we get

$$(1-x^2)F'' + 2xF' - 2F = \Gamma^2 - L^2. \tag{2.15}$$

The system of equations of the ninth order (2.6)–(2.9) and (2.15) has the following boundary conditions:

$$\begin{aligned} &y'(1) = -Re, \quad L(-1) = J, \quad L(1) = 0, \\ &F(\pm 1) = 0, \quad \Gamma(\pm 1) = 0, \quad \Phi(\pm 1) = 0. \end{aligned} \tag{2.16}$$

It follows from (2.6) that the conditions $y(\pm 1) = 0$ are satisfied automatically.

The system of (2.6)–(2.9) and (2.15) with the boundary conditions (2.16) allows solutions with $\Phi = \Gamma = 0$, i.e. $u_\varphi = B_r = B_\theta = 0$, which corresponds to the jet flow without rotation. The possibility of the rotation is studied in § 6.

Equations (2.6)–(2.9) and (2.15) are of Legendre type (Tribel 1978). They have singular points $x = \pm 1$ due to $(1 - x^2)$ factor at the higher derivative. Thus, it is necessary to analyse the equations in the vicinity of singular points and create an algorithm to solve the system since the boundary conditions are non-standard.

3. Analysis of the solution in the vicinity of singular points $x = \pm 1$

Let us find out how functions of (2.6)–(2.9) and (2.15) with the boundary conditions (2.16) behave in the vicinity of the point $x = -1$. First, we consider the situation when $Bt = 0$ and $\Phi = \Gamma = 0$. Then the equations reduce as

$$(1-x^2)y' + 2xy - y^2/2 = F, \tag{3.1}$$

$$(1-x^2)L'' = 0, \tag{3.2}$$

https://doi.org/10.1017/jfm.2014.103 Published online by Cambridge University Press

$$(1-x^2)F'' + 2xF' - 2F = -L^2. \tag{3.3}$$

Taking into account the boundary conditions (2.16), from (3.2) we obtain

$$L = J(1-x)/2. \tag{3.4}$$

Equation (3.3) is solved as follows with regard to the above result. Using this relation for L, equation (3.3) gives

$$F = \frac{J^2}{4}\left((1-x^2) + (1+x)^2 \ln\frac{1+x}{2}\right). \tag{3.5}$$

We see that F is non-analytic at $x=-1$, so is y due to (3.1).

Now let us study a general case $Bt \neq 0$ and $\Gamma \neq 0$, $\Phi \neq 0$. We start with (2.15). Since $L(-1) = J$ and $F(-1) = 0$, we obtain

$$2\epsilon F'' - 2F' = -J^2 + o(1).$$

Thus, $F = \epsilon J^2/2 + o(\epsilon)$, assuming $\epsilon = 1 + x \to +0$. We substitute the expression for F in (3.1) and using that the term $y^2/2$ is of the second order of smallness we obtain

$$2\epsilon y' - 2y = \epsilon J^2/2 + o(\epsilon).$$

Therefore, $y = (y_{10} + J^2(\ln\epsilon)/4)\epsilon + o(\epsilon)$, where y_{10} is the integration constant. Hence, y' has a logarithmic singularity at $x=-1$, with its coefficient determined by J. Note that similar singularity is observed in conical flows in the vicinity of the vortex line (Serrin 1972; Goldshtik 1979; Sozou, Wilkinson & Shtern 1994). The appearance of the $\epsilon \ln\epsilon$ term in the expansion of y suggests that logarithmic terms will also arise in the expansions of other dependent variables.

Similarly, we can obtain the expansion of y, F, L, Γ and Φ up to the ϵ^2 terms. Moreover, we can also get higher orders of the expansion, represented by the remainder

$$\begin{aligned}
y &= (y_{10} + J^2(\ln\epsilon)/4)\epsilon + (y_{20} + y_{21}\ln\epsilon + y_{22}\ln^2\epsilon - BtJ^4(\ln^3\epsilon)/192)\epsilon^2 \\
&\quad + O(\epsilon^3\ln^4\epsilon), && (3.6)\\
F &= J^2\epsilon/2 + (f_{20} + f_{21}\ln\epsilon + f_{22}\ln^2\epsilon - BtJ^4(\ln^3\epsilon)/96)\epsilon^2 + O(\epsilon^3\ln^4\epsilon), && (3.7)\\
L &= J + (L_{10} + L_{11}\ln\epsilon + BtJ^3(\ln^2\epsilon)/16)\epsilon \\
&\quad + (L_{20} + L_{21}\ln\epsilon + L_{22}\ln^2\epsilon + Bt^2J^5(\ln^3\epsilon)/256)\epsilon^2 + O(\epsilon^3\ln^5\epsilon), && (3.8)\\
\Gamma &= \gamma_{10}\epsilon + (\gamma_{20} + \gamma_{21}\ln\epsilon + \gamma_{22}\ln^2\epsilon)\epsilon^2 + O(\epsilon^3\ln^3\epsilon), && (3.9)\\
\Phi &= \phi_{10}\epsilon + \phi_{20}\epsilon^2 + O(\epsilon^3\ln^3\epsilon). && (3.10)
\end{aligned}$$

Substituting (3.6)–(3.10) in (2.6)–(2.9) and (2.15) and combining terms with equal powers of ϵ and $\ln\epsilon$, we express all coefficients by y_{10}, y_{20}, L_{10}, γ_{10} and ϕ_{10} (see appendix B).

The solution should be analytic in the flow region, thus we can expand it in Taylor series about the point $x=1$:

$$\begin{aligned}
y &= Re(1-x) + y_2(1-x)^2 + O((1-x)^3), && (3.11)\\
L &= L_1(1-x) + L_2(1-x)^2 + O((1-x)^3), && (3.12)\\
F &= f_2(1-x)^2 + O((1-x)^3), && (3.13)
\end{aligned}$$

https://doi.org/10.1017/jfm.2014.103 Published online by Cambridge University Press

$$\Gamma = \gamma_1(1-x) + \gamma_2(1-x)^2 + O((1-x)^3), \tag{3.14}$$

$$\Phi = \phi_1(1-x) + O((1-x)^3). \tag{3.15}$$

All of the coefficients of (3.11)–(3.15) depend on L_1, f_2, γ_1 and ϕ_1 (see appendix B).

The values y_{10}, y_{20}, L_{10}, γ_{10} and ϕ_{10} (at $x=-1$) and L_1, γ_1, ϕ_1 and f_2 (at $x=1$) can be determined by matching asymptotic expansions with numerical solution. Using the expansions (3.11)–(3.15) a solution may be obtained starting from the neighbourhood of $x=1$. The functions and their derivatives of the solution should coincide with the functions due to the expansions (3.6)–(3.10) in a certain point of the neighbourhood of $x=-1$. These nine conditions according to the order of the system of (2.6)–(2.9) and (2.15) determine all nine coefficients. This algorithm allows us to use standard methods for the calculation of ordinary differential equations.

4. Non-swirling MHD jet

Let us consider the jet with no swirl when $\Phi = \Gamma = 0$. Then the system of (2.6)–(2.9) and (2.15) takes the form

$$(1-x^2)y' + 2xy - y^2/2 = F, \tag{4.1}$$

$$(1-x^2)L'' = Bt(yL' + 2y'L + 2xyL/(1-x^2)), \tag{4.2}$$

$$(1-x^2)F'' + 2xF' - 2F = -L^2, \tag{4.3}$$

while the boundary conditions (2.16), respectively,

$$y'(1) = -Re, \quad L(-1) = J, \quad L(1) = 0, \quad F(\pm 1) = 0. \tag{4.4}$$

In the case $J=0$, which corresponds to $L=F=0$, y is the analytic function which is the Slezkin–Landau–Squire solution. This solution has the following form

$$y = y_L = \frac{2Re(1-x^2)}{4 + Re(1-x)} \tag{4.5}$$

with two important limits

$$y_L = \begin{cases} 2(1-x), & -1 < x \leqslant 1, \ \ y_L(-1) = 0, \ \ Re \to -2 + 0, \\ 2(1+x), & -1 \leqslant x < 1, \ \ y_L(1) = 0, \ \ Re \to \infty. \end{cases} \tag{4.6}$$

The above limiting solutions correspond to jets with an infinite momentum flowing in opposite directions.

4.1. *Method of computation*

Here we describe in detail the computational routine used to solve (4.1)–(4.3). We have five coefficients to determine: y_{10}, y_{20}, L_{10} (at $x=-1$) and f_2, L_1 (at $x=1$). The parameters of the problem are Re, J and Bt. First, we set Re, Bt and L_1 (instead of J). A boundary value problem is specified for each $L_1 = -L'(1)$ and certain $f_2 = F''(-1)/2$, which gives one solution with specific J (table 1). We build a numerical solution, with the integration starting from $x = x_p$, which is close to $x = 1$, using the expansions (3.11)–(3.13) at $x = x_p$. We choose x_p according to the computational accuracy as

https://doi.org/10.1017/jfm.2014.103 Published online by Cambridge University Press

L_1	f_2	y_{10}	y_{20}	L_{10}	J
0	0	1.66667	−0.13888	0	0
1	0.05587	1.91853	−0.32609	0.31445	0.68240
1.5	0.12662	2.25641	−0.62764	0.92669	1.04654
2	0.22761	2.78161	−1.18658	2.20391	1.44367
2.5	0.36147	3.57616	−2.15192	4.65466	1.89774
3	0.53341	4.83250	−3.61593	9.37085	2.45793
3.5	0.75678	7.17990	−4.14803	19.73918	3.26772
3.942	1.09132	17.47199	95.53818	71.25771	5.53524
3.5	1.11792	75.60035	5.363×10^3	452.54941	11.03825
3	1.01079	214.42940	4.628×10^4	2.216×10^3	17.09002
2.5	0.89361	637.20425	3.606×10^5	1.343×10^4	26.72215
2	0.78096	2.185×10^3	3.336×10^6	1.030×10^5	44.53655
1.5	0.67972	9.690×10^3	4.341×10^7	1.154×10^6	83.61568
1	0.59486	6.828×10^4	9.209×10^8	2.550×10^7	195.45607

TABLE 1. Coefficients of the expansions. Non-swirling jet. Here $Re = 10$ and $Bt = 1$. There are two solutions for each value of L_1, which corresponds to the confinement of the current density described below.

described below. The numerical solution is to satisfy five conditions according to the order of (4.1)–(4.3)

$$y(x_{c1}) = y_-(x_{c1}), \quad L(x_{c1}) = L_-(x_{c1}), \quad L'(x_{c1}) = L'_-(x_{c1}),$$
$$F(x_{c1}) = F_-(x_{c1}), \quad F'(x_{c1}) = F'_-(x_{c1}), \tag{4.7}$$

where x_{c1} is close to $x = -1$. The subscript '$-$' denotes the expansions (3.6)–(3.8) (at $x = -1$). As the result, we obtain the full set (f_2, y_{10}, y_{20}, L_{10}, J) as the function of (L_1, Re, Bt). Table 1 shows some values for coefficients. We use a set (f_2^s, y_{10}^s, y_{20}^s, L_{10}^s, J^s) as the starting point, where the superscript 's' shows that these values have to be close to the exact ones so that the condition (4.7) has a proper convergence of the Newton method used. To find the starting point for (4.7), we build a numerical solution which satisfies the approximate boundary condition

$$y(x_{c2}) = 0, \tag{4.8}$$

where x_{c2} is also close to $x = -1$ and $x_{c2} < x_{c1}$. Therefore, from (4.8) we find the value $f_2 = f_2^s$ which is close to the exact one. Next we determine four values $y_{10} = y_{10}^s$, $y_{20} = y_{20}^s$, $L_{10} = L_{10}^s$, and $J = J^s$ from four algebraic conditions

$$y(x_{c1}) = y_-(x_{c1}), \quad L(x_{c1}) = L_-(x_{c1}), \quad L'(x_{c1}) = L'_-(x_{c1}), \quad F(x_{c1}) = F_-(x_{c1}), \tag{4.9}$$

using the same solution with $f_2 = f_2^s$.

The numerical calculations were performed using the Runge–Kutta method of the ninth order with automatic selection of the step. The conditions (4.7), (4.8) and (4.9) were satisfied using the Newton method. The computational accuracy was set higher or equal to the value of the neglected terms in the expansions (3.6)–(3.8) (at $x = -1$) (if the expansions were used up to ϵ^2 terms, then ϵ^3 were the neglected terms) and in the expansions (3.11)–(3.13) (at $x = 1$). When the coefficients were obtained, the asymptotic expansions were examined to verify their adequacy (see figures 2*b* and 5*b*). The relative error was estimated by the value of the smallest term in the expansions (3.6)–(3.8) and did not exceed 10^{-9}.

https://doi.org/10.1017/jfm.2014.103 Published online by Cambridge University Press

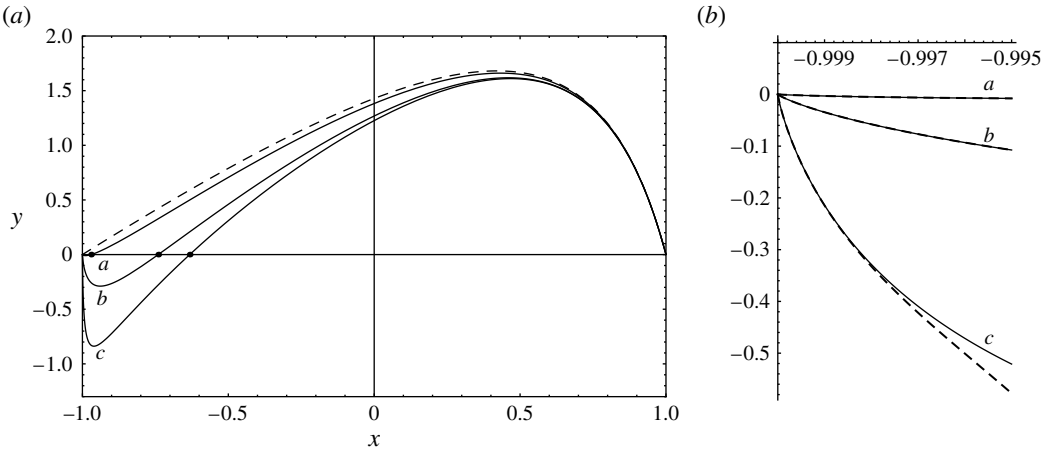


FIGURE 2. Changes in $y(x)$ with the increase in J. Non-swirling jet. Here $Re = 10$ and $Bt = 1$. (*a*) Dashed line is used to show the Slezkin–Landau–Squire solution (4.5). The curves a, b and c correspond to $J_a = 2$, $J_b = 5.54$ and $J_c = 15.68$. The function $y(x)$ becomes zero if $x_a = -0.97$, $x_b = -0.74$ and $x_c = -0.63$. (*b*) Solid lines show the numerical calculation, while dashed lines indicate the expansion of $y(x)$ (3.6). With the increase in J asymptotic expansions are valid as the vicinity of the point $x = -1$ becomes smaller.

4.2. *Reverse flow*

Figure 2 shows the graphs of y at various values of J. According to (3.6), y ceases to be a non-negative function for $J > 0$, because $y(-1) = 0$ and $y' < 0$ if $x \to -1$, i.e. a reverse flow occurs along the wire, and its boundary is determined by the zero of y. The stream function $\psi = \nu r y$ is presented in figure 3. Apart from the increase in the reverse flow region with J, it is also important to note that a significant crowding of the streamlines occurs in the vicinity of the wire.

We consider the behaviour of the forces in order to analyse the reverse flow region. A distinctive feature of the problem is the influence of the Lorentz force. This force has the form

$$\boldsymbol{F}_b = \boldsymbol{j} \times \boldsymbol{B} = \boldsymbol{B} \cdot \nabla \boldsymbol{B}/\mu - \nabla(\boldsymbol{B}^2/2\mu).$$

In compliance with (2.5) and (2.14) the Lorentz force is

$$\boldsymbol{F}_b = \frac{\rho \nu^2}{r^3}\left(-\Phi\Phi''\boldsymbol{e}_r + \left(\frac{LL'}{\sqrt{1-x^2}} + \sqrt{1-x^2}\Phi'\Phi''\right)\boldsymbol{e}_\theta + \frac{\Phi L'}{\sqrt{1-x^2}}\boldsymbol{e}_\phi\right)$$

and has only θ component if $\Phi = 0$. Then the Lorentz force, being negative in almost the entire flow region, is positive in a small neighbourhood of $x = -1$ ($L > 0$ and $L' > 0$ if $x \to -1$, see figure 5*b*), where it drives the fluid to the wire.

Let us analyse the cumulative effect of the forces. We consider the total pressure p_t that is the sum of the hydrodynamic and magnetic pressure. According to (2.5), we obtain

$$p_t = p + \frac{\boldsymbol{B}^2}{2\mu} = p_\infty + \frac{\rho \nu^2}{r^2} p_0(x), \quad p_0 = \frac{1}{1-x^2}(2xy - y^2 - xF' + \Phi^2).$$

https://doi.org/10.1017/jfm.2014.103 Published online by Cambridge University Press

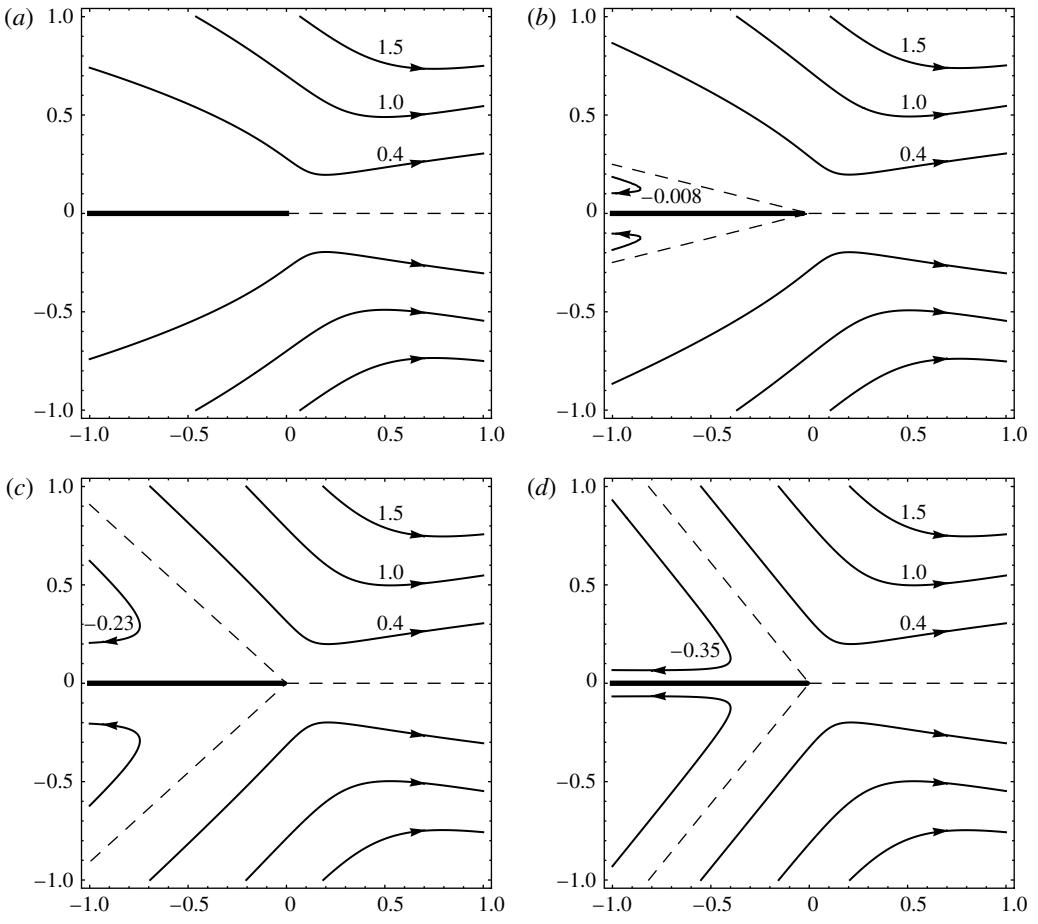


FIGURE 3. Graph of the stream function $\psi/\nu = ry(x)$. Here $Re = 10$ and $Bt = 1$: (*a*) $J = 0$; (*b*) $J = J_a$; (*c*) $J = J_b$; (*d*) $J = J_c$. Dashed lines mark the region with $\psi = y = 0$.

Using the expansions (3.6)–(3.10), in the vicinity of the wire

$$p_0 = \frac{J^2}{4\epsilon} - \frac{BtJ^4}{96}\ln^3\epsilon + o(\ln^3\epsilon), \quad \epsilon = 1 + x \to +0.$$

We see that the point $x = -1$ is a simple pole of p_0. Note that the semi-infinite vortex line produces the same simple pole for the pressure function (see Sozou *et al.* (1994, equation 11)). As a result, the axial momentum

$$P_z = 2\pi r^2 \int_0^\pi (\Pi_{rr}\cos\theta - \Pi_{r\theta}\sin\theta)\sin\theta\,\mathrm{d}\theta \tag{4.10}$$

is logarithmically infinite for all Re numbers.

We consider the balance of viscous, pressure and Lorentz forces in the MHD equations. The sum of three forces gives the following result in the third order for the radial inertial force

$$F_r = \rho(\boldsymbol{u}\cdot\nabla\boldsymbol{u})_r = -\frac{\rho\nu^2}{r^3}\left(\frac{J^4}{16}\ln^2\epsilon + \frac{J^2}{2}\left(\frac{3J^2}{8} + y_{10}\right)\ln\epsilon\right.$$

https://doi.org/10.1017/jfm.2014.103 Published online by Cambridge University Press

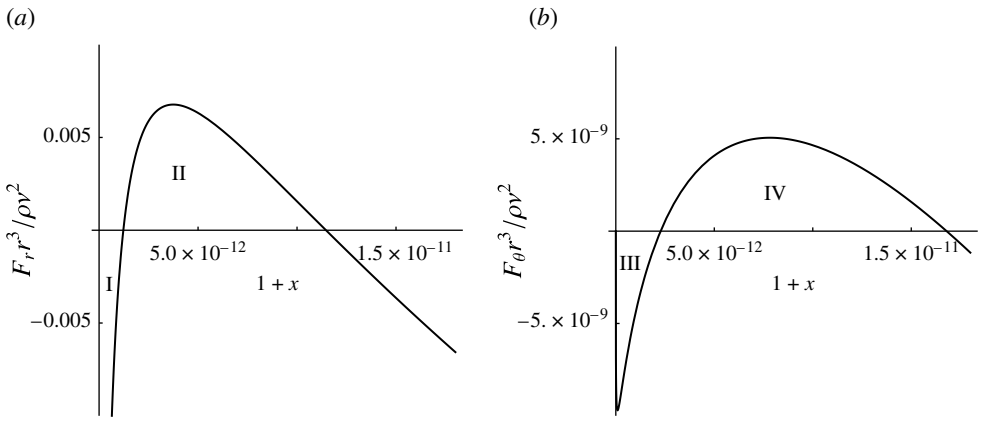


FIGURE 4. Graph of the radial F_r and poloidal F_θ inertial force. Non-swirling jet. Here $Re = 10$, $J = 0.54$ and $Bt = 1$. Here $y_{10} = 1.83$, $y_{20} = -0.25$, $L_{10} = 0.19$, $f_2 = 0.04$, $L_1 = 0.80$ and $\gamma_{10} = \phi_{10} = 0$. (*a*) Expression of F_r according to formula (4.11). In region I the radial force is directed towards the origin, and in region II from the origin. (*b*) Expression of F_θ according to formula (4.12). In region III the force is directed from the wire, in region IV towards the wire. Unlike regions I and III, regions II and IV grow significantly with the increase in J, which causes reverse flow.

$$+\frac{1}{16}(J^4 + 12J^2 y_{10} + 16y_{10}^2) + o(1)\Big), \tag{4.11}$$

and poloidal inertial force gives the result in the sixth order

$$F_\theta = \rho(\boldsymbol{u}\cdot\nabla\boldsymbol{u})_\theta = -\frac{\rho\nu^2}{r^3}\sqrt{\frac{\epsilon}{8}}\left(\frac{J^4}{16}\ln^2\epsilon + \frac{J^2}{8}(J^2 + 4y_{10})\ln\epsilon + \left(-\frac{1}{2}J^2 y_{10} - y_{10}^2 + \gamma_{10}^2\right) + o(1)\right). \tag{4.12}$$

Figure 4 shows the graphs of F_r and F_θ, according to (4.11) and (4.12). As may be seen, at $x \to -1$ the inertial force is negative. Thus, the sum of the forces is directed towards the origin and from the wire. However, an expanding region with positive values of the inertial force occurs in the immediate vicinity of $x = -1$ (regions II and IV), which drives the fluid to the wire and pushes it away from the origin. Then the region of the reverse flow starts to expand with the increase in J, but upon reaching certain values, its changes become less significant (see figure 3).

4.3. *Current confinement*

With the increase in J from zero to a certain value J_m the current density j_r increases in every point of the space $-1 < x \leqslant 1$. Next, if $J > J_m$, j_r starts to decrease monotonically in the right half-space ($x \geqslant 0$) and tends to zero, concentrating in the vicinity of the wire. Figure 5*a* shows the behaviour of the current density on the semi-axis $x = 1$ with the change in J or, according to (2.14), dependence of $L'(1)$ on J. The point b corresponds to the current value J_m, at which the current density is maximum and $L'(1) = -3.942$. Therefore, with the increase in J there are fewer

https://doi.org/10.1017/jfm.2014.103 Published online by Cambridge University Press

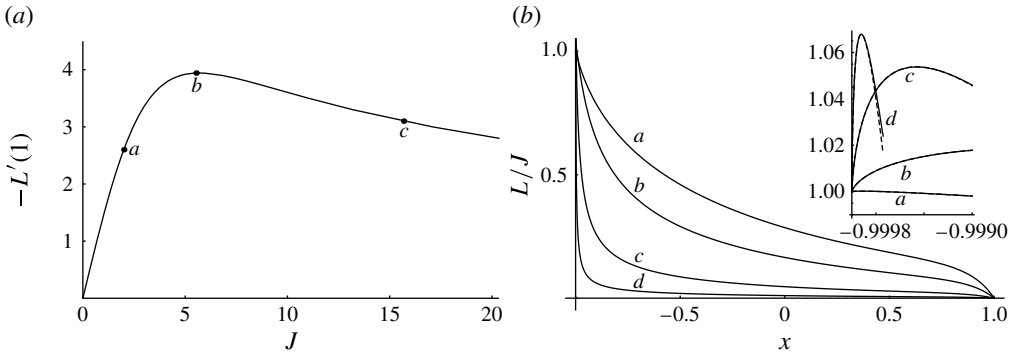


FIGURE 5. Non-swirling jet. Here $Re = 10$ and $Bt = 1$. (*a*) The behaviour of the current density on the semi-axis $x = 1$ with the change of J. Note that $L'(1) = -L_1$. The letters a, b and c correspond to the current values J_a, J_b and J_c, respectively. (*b*) Graph of L normalized by J. The curve d corresponds to $J_d = 44.54$. In the inset solid lines show the numerical calculation, which virtually coincide with dashed lines indicating the expansion of L (3.8). Note that $L' > 0$ if $x \to -1$, according to (3.8).

electrical charges in the right half-space where the jet propagates, i.e. the current is blocked in the direction of the jet. The distribution of the current is illustrated by figure 5*b*, showing the dependence L/J, which is a part of the current discharged in a spherical segment $[x, 1]$ or $0 \leqslant \theta \leqslant \arccos(x)$.

4.4. *Existence of the solution*

Investigating the dependence of the numerical solution on Re, J and Bt we find the following. When $Bt = 0$, the solution of (4.1)–(4.3) appears to exist only at specific values of J. At certain finite values of $J = J_\infty(Re)$ a strong jet is formed on the semi-axis $x = -1$ leading to the breakdown of the solution (collapse).

If $Bt = 0$, then according to (4.1)–(4.3), the equation reads

$$(1-x^2)y' + 2xy - \frac{y^2}{2} = \frac{J^2}{4}\left((1-x^2) + (1+x)^2 \ln\frac{1+x}{2}\right). \tag{4.13}$$

To find the solution we use a simplified version of the computational algorithm described in § 4.1. Only one coefficient y_{10} remains indeterminate. We match the condition: $y(x_{c2}) = y_-(x_{c2})$, where y is the numerical solution and the subscript '$-$' denotes the expansion (3.11).

For a fixed Re when increasing J up to J_∞ the value of y_{10} tends to infinity. When $J = J_\infty$, the function y obtains a singularity at $x = -1$; thus, the boundary condition $y(-1) = 0$ cannot be satisfied (figure 6*a*). This singularity of the solution is not preserved at non-zero values of Bt. Figure 6*b* shows that if $Bt \neq 0$ the minimum of y near the wire (figures 2*a* and 6*a*) approaches $x = -1$ as $J^{-1/f(Bt)}$. The general behaviour of f is addressed in the next paragraph, while at small Bt it can be approximated as $f(Bt) = 2Bt$ manifesting the breakdown of the solution at finite J for $Bt = 0$.

5. Boundary-layer solutions

Figure 6*a* suggests that there are solutions of the boundary-layer type near $x = -1$. Similar solutions for y are typical of $Bt \neq 0$ and large J. Here we study the behaviour

https://doi.org/10.1017/jfm.2014.103 Published online by Cambridge University Press

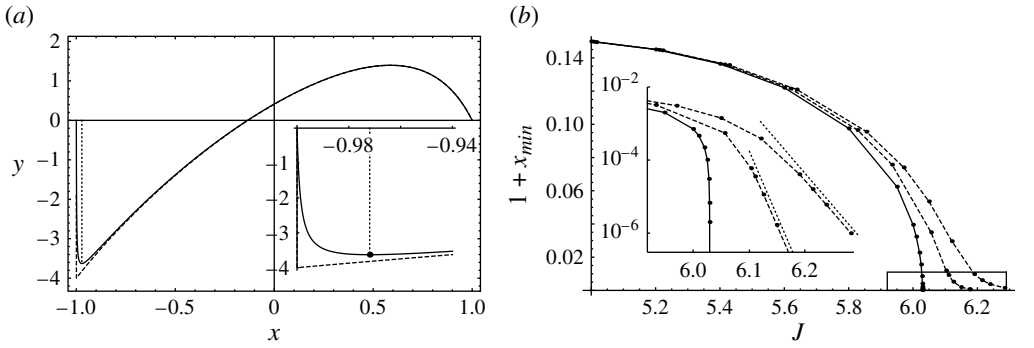


FIGURE 6. Non-swirling jet. Here $Re = 10$. (*a*) When $Bt = 0$, graphs of $y(x)$. The solid line marks the solution for $J = 6.015$, while the dashed line corresponds to $J = 6.02928$, which is very close to J_∞. The vertical dotted line indicates the point $x = x_{min}$, where y reaches its minimum value. (*b*) Graph of $(1 + x_{min})$ depending on J for various Bt. The solid line corresponds to $Bt = 0$, the dashed lines show $Bt = 0.001$ and 0.002 (from left to right). The inset region is framed for convenience. Dotted lines denote functions proportional to $J^{-1/f(Bt)}$, where $f(Bt) = 2Bt$.

of the solution when J tends to infinity. We use two equations for y and L instead of (4.1)–(4.3):

$$(1-x^2)^2 y''' - (1-x^2)(y''y + y'^2) - 2xyy' + y^2 = -L^2, \tag{5.1}$$

$$(1-x^2)L'' = Bt(yL' + 2y'L + 2xyL/(1-x^2)). \tag{5.2}$$

To examine the boundary layer near the wire it is convenient to introduce the inner coordinate η. For large Bt ($Bt > 1/2$ as shown below), we define $\eta = J^\beta(1+x)$ following Goldshtik & Shtern (1989) who introduced the inner variable studying a flow near a conical surface at high Reynolds numbers. The only choice of η which retains the term L^2 in the equation for y is $\beta = 2$; it makes the effect of the magnetic field on hydrodynamics non-negligible. Using this boundary layer scaling in (5.1) and (5.2), we neglect terms of lower orders of J^2 and normalize $L_0 = L/J$

$$2\eta^2 y_0''' - \eta(y_0'^2 + y_0 y_0'') + y_0 y_0' = -L_0^2/4, \tag{5.3}$$

$$\eta L_0'' = Bt(y_0 L_0' + 2y_0' L_0 - y_0 L_0/\eta). \tag{5.4}$$

The boundary conditions on the axis (wire) are $y_0(0) = 0$ and $L_0(0) = 1$. The inner solution should match the outer one if η tends to infinity, thus $y_0(\infty) = y_\infty$ and $L_0(\infty) = 0$. To build a numerical solution of (5.3) and (5.4) we use the previously described technique (§ 4.1). We calculate asymptotic expansions in the vicinity of $\eta = 0$ for y_0 and L_0 which possess the same logarithmic singularity as y and L in (3.6) and (3.8):

$$y_0 = \eta(y_{10} + y_{11}\ln\eta) + \eta^2(y_{20} + y_{21}\ln\eta + y_{23}\ln^2\eta) + o(\eta^2), \tag{5.5}$$

$$L_0 = 1 + \eta(L_{10} + L_{11}\ln\eta + L_{12}\ln^2\eta) + \eta^2(L_{20} + L_{21}\ln\eta + L_{22}\ln^2\eta + L_{23}\ln^3\eta) + o(\eta^2), \tag{5.6}$$

and compute $y_0(\eta_p)$, $y_0'(\eta_p)$, $y_0''(\eta_p)$, $L_0(\eta_p)$ and $L_0'(\eta_p)$, where η_p is close to $\eta = 0$. Then the numerical integration of (5.3) and (5.4) is performed from $\eta = \eta_p$ to η_c, with η_p

https://doi.org/10.1017/jfm.2014.103 Published online by Cambridge University Press

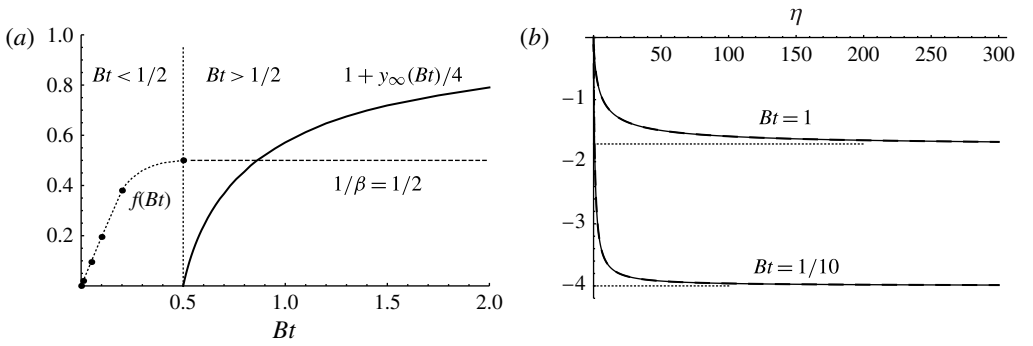


FIGURE 7. (*a*) The solid line marks the dependence of the coefficient y_∞ on Bt. For $Bt \to 1/2 + 0$, y_∞ approaches -4, while for large Bt, y_∞ tends to zero. Dots (connected by the dotted line) are the values of $f(Bt)$ calculated as in figure 6*b*. Function f behaves as $2Bt$ for small Bt, while for $Bt \to 1/2 - 0$, $f \to 1/2 - 0$, which is equal to $\beta = 2$ (dashed line). (*b*) Graph of y. The comparison between the exact (for $Re = 10$) and boundary-layer solution. The solid lines mark two exact solutions ($Bt = 0.1$, $J = 193.66$; $Bt = 1$, $J = 1.24 \times 10^6$). The dashed lines show (5.9) for $Bt = 0.1$ and the boundary-layer solution of (5.3) and (5.4) for $Bt = 1$.

and η_c being the points where asymptotic expansions of y_0 and L_0 are valid in the vicinity of $\eta = 0$ and $\eta = \infty$ correspondingly. Note that if $\eta = \infty$, (5.4) suggests the power law expansion for L_0 and, as a consequence, for y_0. These expansions have the form

$$y_0 = y_\infty + y_1 \eta^{1+Bty_\infty} + y_2 \eta^{2(1+Bty_\infty)} + o(\eta^{2(1+Bty_\infty)}), \tag{5.7}$$

$$L_0 = L_1 \eta^{Bty_\infty/2} + L_2 \eta^{1+3Bty_\infty/2} + L_3 \eta^{2+5Bty_\infty/2} + o(\eta^{2+5Bty_\infty/2}). \tag{5.8}$$

The coefficients y_{10}, y_{20}, L_{10}, y_∞ and L_1 are to be determined. Starting the integration of (5.3) and (5.4) from $\eta = \eta_p$, we match $y_0(\eta_c)$, $y_0'(\eta_c)$, $y_0''(\eta_c)$, $L_0(\eta_c)$ and $L_0'(\eta_c)$ with (5.7) and (5.8). The behaviour of $y_\infty(Bt)$ is shown in figure 7*a*. Note that the solution of (5.3) and (5.4) cannot be obtained for $Bt = 1/2$ since $(2Bt - 1)$ expression appears in the denominator of some coefficients of (5.7) and (5.8) (see appendix D). Figure 7*b* shows that the exact and boundary-layer solutions are indistinguishable for both cases ($Bt > 1/2$ and $Bt < 1/2$) with the last one described below.

For Bt smaller than $1/2$ another scaling for η is needed. As mentioned above, $(1 + x_{min})$ approaches zero as $J^{-1/f(Bt)}$, where $f(Bt)$ is shown in figure 7*a*. It is natural to use the scaling $\eta = J^{1/f}(1 + x)$. If Bt tends to $1/2$ the previously used dependence $\eta \sim J^2$ is recovered. With the new scaling for $Bt < 1/2$ the term on the right-hand side of (5.3) is to be neglected which means that the magnetic field has low impact. The obtained equation has the exact solution of the Slezkin–Landau–Squire type:

$$y_0 = -\frac{4\eta}{C_0 + \eta}, \tag{5.9}$$

where parameter C_0 can be adopted as 1 without loss of generality.

6. Swirling MHD jet

Following from (2.6)–(2.9) and (2.15), non-zero azimuthal velocity may occur due to the poloidal magnetic field. It may be attributed to the effect of the Lorentz force

https://doi.org/10.1017/jfm.2014.103 Published online by Cambridge University Press

γ_1	$-\phi_1$	L_1	f_2	y_{10}	y_{20}	L_{10}	J	$-\phi_{10}$	γ_{10}
0	0	3.57	1.13	65.35	3.9×10^3	370.12	10.36	0	0
5.82	1.25	8.92	0.94	146.47	1.5×10^4	1.6×10^3	14.05	4.77	50.95
9.90	1.64	16.94	3.41	369.10	7.8×10^4	7.2×10^3	20.32	10.76	173.65
13.23	1.82	23.89	8.09	832.79	3.5×10^5	2.6×10^4	28.49	19.18	460.49
17.8	1.73	31.67	15.14	2.7×10^3	2.8×10^6	1.7×10^5	46.69	40.20	1.7×10^3

TABLE 2. Coefficients of the expansions. Swirling jet. Here $Re = 10$ and $Bt = 1$.

which obtains a rotational component in this case. Therefore, the poloidal magnetic field indicates spontaneous rotation. This section is dedicated to the study of the possible bifurcation of the poloidal magnetic field if key parameters of the MHD flow are changed.

Let us find the conditions which stipulate the appearance of $u_\varphi \neq 0$. In the linear approximation of Φ and Γ the problem reduces to finding non-trivial solutions of (2.8) with y found from (4.1) to (4.3). As follows from (2.7), $\Phi \neq 0$ leads to $\Gamma \neq 0$. In fact, two new solutions appear that differ only in the sign.

The solution of the full system of (2.6)–(2.9) and (2.15) is found by a method similar to that described in § 4.1. Instead of $L'(1)$ and (4.8), we set $\Gamma'(1) = -\gamma_1$ to find the solution with rotation, then we satisfy three approximate boundary conditions

$$y(x_{c1}) = 0, \quad \Gamma(x_{c1}) = 0, \quad \Phi(x_{c1}) = 0, \tag{6.1}$$

obtaining (L_1^s, f_2^s, ϕ_1^s). When γ_1 is small (then ϕ_1 is also small) the values of L_1 and f_2 for the non-swirling problem can be used as the starting point for (6.1). Next we obtain $(y_{10}^s, y_{20}^s, L_{10}^s, J^s, \gamma_{10}^s, \phi_{10}^s)$ satisfying

$$\begin{aligned} &y(x_{c2}) = y_-(x_{c2}), \quad L(x_{c2}) = L_-(x_{c2}), \quad L'(x_{c2}) = L'_-(x_{c2}), \\ &F(x_{c2}) = F_-(x_{c2}), \quad \Gamma(x_{c2}) = \Gamma_-(x_{c2}), \quad \Phi(x_{c2}) = \Phi_-(x_{c2}). \end{aligned} \tag{6.2}$$

After all of the values for the starting point are obtained, we solve the following system

$$\begin{aligned} &y(x_{c2}) = y_-(x_{c2}), \quad L(x_{c2}) = L_-(x_{c2}), \quad L'(x_{c2}) = L'_-(x_{c2}), \\ &F(x_{c2}) = F_-(x_{c2}), \quad F'(x_{c2}) = F'_-(x_{c2}), \quad \Gamma(x_{c2}) = \Gamma_-(x_{c2}), \\ &\Gamma'(x_{c2}) = \Gamma'_-(x_{c2}), \quad \Phi(x_{c2}) = \Phi_-(x_{c2}), \quad \Phi'(x_{c2}) = \Phi'_-(x_{c2}). \end{aligned} \tag{6.3}$$

Then all nine coefficients are defined. Some results are presented in table 2.

At small values of J, $\Phi = \Gamma = 0$, i.e. the solution exists only for the non-swirling jet. At $J = J_{bif}$ there is a pitchfork bifurcation of the solution with $\Phi \neq 0$ and $\Gamma \neq 0$ (see figure 8*a*). According to the general theory (Arnold *et al.* 1999), a new solution with rotation is expected to be stable, while the previous solution without rotation is likely to lose stability. For the swirling jet the confinement of the current density described for the non-swirling jet does not exist. The reason is the decrease in the reverse flow region with the increase in J, which reduces the effect. Thus, the rotation of the fluid eliminates the current confinement effect.

Figure 8*b* shows the surface in the space of parameters Re, J and Bt, below which there is only one solution of (2.6)–(2.9) and (2.15) for the non-swirling jet, while

https://doi.org/10.1017/jfm.2014.103 Published online by Cambridge University Press

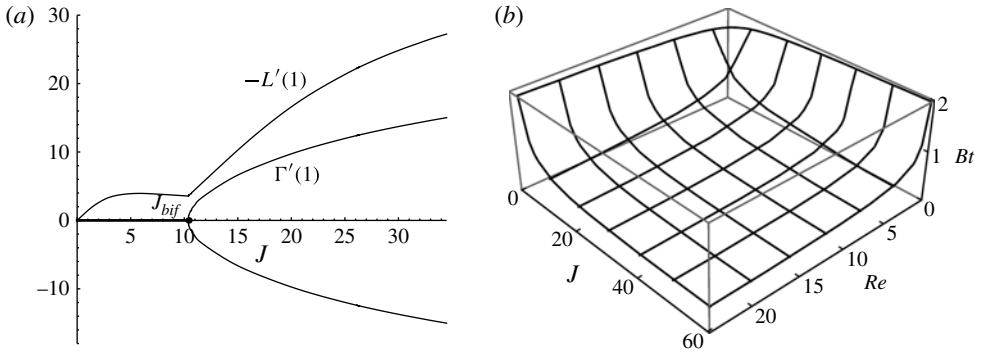


FIGURE 8. (*a*) Graph of $\Gamma'(1)$ and $L'(1)$ of J. Here $\Gamma'(1) = -\gamma_1$ is selected as a bifurcation parameter. Here $Re = 10$ and $Bt = 1$. Here $J = J_{bif} = 10.36$ is the point where the solution for the non-swirling jet bifurcates into two solutions with $\Gamma \neq 0$ and $\Phi \neq 0$. (*b*) Graph of the surface in the parameter space (Re, J, Bt). The solution for the non-swirling jet exists below this surface. There are three solutions above the surface: one solution for the non-swirling jet and two for the swirling one.

above it there are three solutions: one solution for the non-swirling jet and two for the swirling one. If a point belongs to the surface, the solution with $\Phi \neq 0$ and $\Gamma \neq 0$ appears.

Let us explain qualitatively the excitation mechanism for the poloidal field. Assume an initial disturbance of the magnetic field to occur along the flow at the point $x = 1$. We consider a torus of liquid particles placed around the wire and perpendicular to it. The flow directed towards the origin advects the torus and compresses it to the axis (figure 3). Thus, magnetic flux through the torus changes and, consequently, an azimuthal current occurs. It induces a magnetic field that has the same direction as the initial one in the region near the axis $x = 1$. Therefore, the chain of causation takes place from the magnetic field to the current and *vice versa*, i.e. positive feedback is formed. However, magnetic diffusivity being high, the increase in the magnetic field is offset by its diffusion. It can be easily seen in figure 8*b*. If we fix one of the flow parameters (for instance, J), then a bifurcation curve appears in the (Re, Bt) plane along which $\mathrm{d}Bt/\mathrm{d}Re < 0$. Hence, for the excitation of the poloidal field to occur with the increase in λ, i.e. decrease in Bt, Re is to be increased. This is true for any pair of the parameters Re, J and Bt. Thus, convergent flow is essential for the excitation of the poloidal field and azimuthal velocity.

7. Discussion

The solution obtained in this paper is the limiting case of the problem considered by Sozou & English (1972). They neglected the no-slip condition on the plane boundary and presented the problem as the interaction of the flow field due to a source of momentum (Squire 1952) with the flow field induced by the point electrode discharging the current. Their solution has a singularity at certain parameters on the axis of symmetry $x = 1$ which corresponds to the case $y'(1) = -Re$, $Re \to \infty$ in our problem. However, Sozou and English did not report about the singularity on the conical wall, while we describe the singularity on the wire $(x = -1)$ in § 4.4. This question is addressed in the end of this section. Another important point is the no-slip

https://doi.org/10.1017/jfm.2014.103 Published online by Cambridge University Press

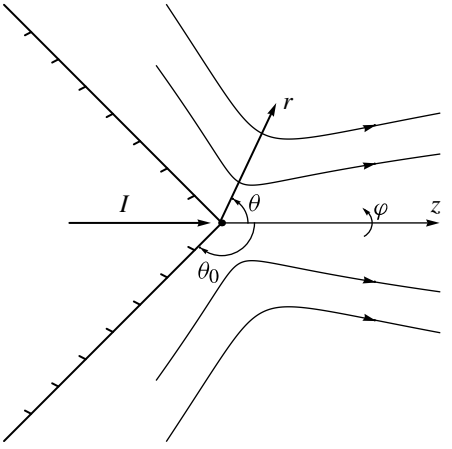


FIGURE 9. Problem scheme for an arbitrary angle θ_0.

condition on the wire. One may ask whether it is significant for the solution to be relevant. We examine the consequences of the no-slip condition below.

Let us briefly revisit the problem considered by Sozou (1971), Narain & Uberoi (1971) and others. The meridional flow is induced by the point electrode discharging the current I (see figure 9). The electrode is placed on the vertex of the cone with insulated infinite walls. The angle between the axis of symmetry and the cone wall is θ_0 $(x_0 = \cos\theta_0)$.

7.1. *No-slip condition on the wall*

To simplify the analysis we consider the case $Bt = 0$. If $\Phi = \Gamma = 0$, the governing equations are (3.1) and (3.3). The boundary conditions are the no-slip condition on the conical wall $y(x_0) = y'(x_0) = 0$ and $F(x_0) = 0$ following from (3.1). On the axis $x = 1$ the same conditions (2.13) and (2.16) are valid, i.e. $y(1) = F(1) = L(1) = 0$. Then, instead of (3.4), we have $L = J(1-x)/(1-x_0)$ since $L(x_0) = J$, which follows from conservation of charge. From (3.3) with the above boundary conditions we obtain an explicit expression

$$F = 2J^2\frac{x-x_0}{(1-x_0)^4}((1-x)(1-x_0) - 2(1-x_0x)\ln 2) + \frac{J^2}{(1-x_0)^2}\left((1+x)^2\ln(1+x) - (1+x_0)^2\left(\frac{1-x}{1-x_0}\right)^2\ln(1+x_0)\right). \quad (7.1)$$

Usually the characteristic of the current magnitude is the dimensionless parameter S defined in § 1. To compare results the relation $S = J^2$ can be used (figure 10).

Let us consider the axial momentum flux through the unit surface of the conical wall. Thus, after a little algebra we have

$$\Pi_{z\theta} = \Pi_{r\theta}\cos\theta - \Pi_{\theta\theta}\sin\theta = \frac{2\rho\nu^2}{r^2\sqrt{1-x^2}}((1-x^2)y' + 2xy - y^2/2 - F), \quad x = x_0, \quad (7.2)$$

https://doi.org/10.1017/jfm.2014.103 Published online by Cambridge University Press

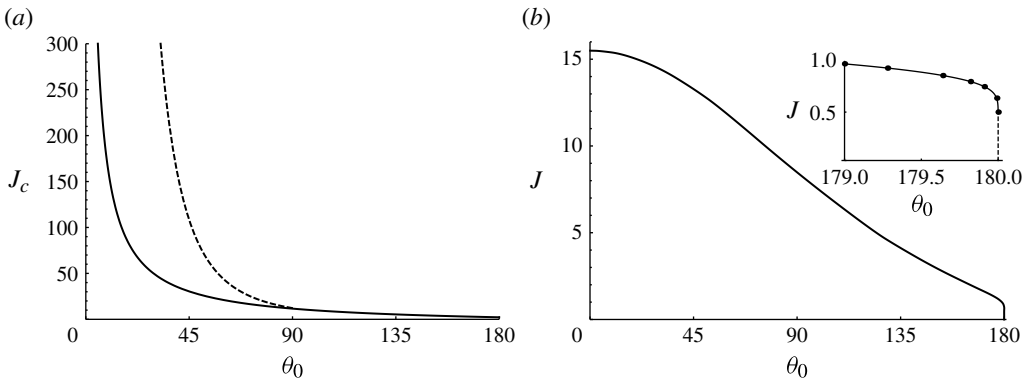


FIGURE 10. Non-swirling jet. (*a*) Graph of the critical value J_c against the angle θ_0 (in degrees). When $J = J_c$ the solution of (3.1) obtains a singularity on the axis $x = 1$, then P_z becomes infinite. The value $J_c = 12.25$ ($S_c = 150$) agrees with that obtained by Sozou (1971) if $\theta_0 = 90°$ ($x_0 = 0$). The solid line corresponds to the numerical results obtained in this paper. The dashed line corresponds to the analytic expression $J_c = 1.7467 \times 10^7 \theta_0^{-3.15}$ derived by Narain & Uberoi (1973). (*b*) Graph of J against θ_0 (in degrees). The numerical calculations are carried out for (3.1) when the value $y'(1) = -Re$ is fixed with $Re = 10$. Here J tends to a finite value if $\theta_0 \to 0°$ ($x_0 \to 1$) and J tends to zero if $\theta_0 \to 180°$ ($x_0 \to -1$) as shown in the text.

which equals zero, since the expression in parentheses is (3.1). This fact does not depend on the boundary conditions on conical walls and can be extended on the case $\Phi \neq 0$ and $\Gamma \neq 0$, then we have (2.6) in parentheses. Thereby, does the Lorentz force determine the flow or is there a mechanical source of motion at the origin determined by the current magnitude? To answer this question the axial momentum (4.10) is calculated

$$P_z = 2\pi r^2 \int_0^{\theta_0} (\Pi_{rr} \cos\theta - \Pi_{r\theta} \sin\theta) \sin\theta \, \mathrm{d}\theta = 2\pi\rho\nu^2 \int_{x_0}^{1} \left(xy'^2 - 4xy' - \frac{2x^2 y}{1-x^2} \right) \mathrm{d}x$$
$$+ 2\pi\rho\nu^2 \int_{x_0}^{1} \frac{xF - x^2 F'}{1-x^2} \, \mathrm{d}x = \rho\nu^2 (I_y + I_f), \tag{7.3}$$

where I_y and I_f are the dimensionless integrals depending on y and F respectively. Using (7.1), another explicit expression can be obtained:

$$I_f = -2\pi J^2 \left(\frac{2x_0^2 + 3x_0 - 1}{(1-x_0)^3} \ln\left(\frac{1+x_0}{2} \right) + \frac{x_0^2 + 10x_0 - 3}{4(1-x_0)^2} \right). \tag{7.4}$$

Here I_f has a logarithmic singularity as $x_0 \to -1$, meanwhile, $I_f = \pi J^2/12$ is finite as $x_0 \to 1$. Apparently, the axial momentum cannot be infinite since the no-slip condition on the wall is set. It is confirmed by numerical calculations which demonstrate that I_f is finite as $x_0 \to -1$ (see figure 11). Thus, $J^2 \ln(1 + x_0)$ tends to a constant value as x_0 tends to -1, with J being a function of x_0 (and a function of $y'(1)$ or Re). In the leading order

$$J = J_0 \ln^{-1/2}(1 + x_0), \tag{7.5}$$

where J_0 is the constant. As a result we obtain that J tends to zero according to (7.5) as x_0 tends to -1, while there is no solution if $x_0 = -1$.

https://doi.org/10.1017/jfm.2014.103 Published online by Cambridge University Press

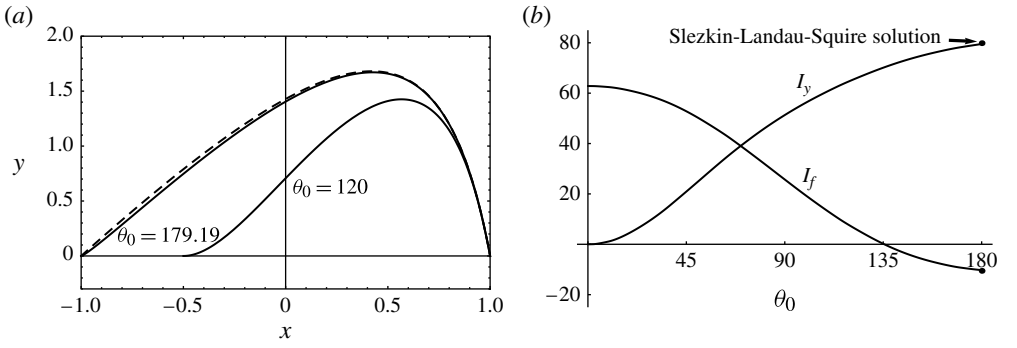


FIGURE 11. Non-swirling jet. (*a*) Graph of $y(x)$. The solid lines correspond to the numerical solutions of (3.1) with $y'(1) = -Re = -10$ for $\theta_0 = 120$ and $\theta_0 = 179.19°$, then $J = 5.41$ and $J = 0.97$, respectively. The dashed line marks the Slezkin–Landau–Squire solution (4.5). As $\theta_0 \to 180°$, the solution of (3.1) tends to the Slezkin–Landau–Squire solution. (*b*) Graph of I_y and I_f defined by (7.3) and (7.4). Here I_y tends to the value for the Slezkin–Landau–Squire solution as $\theta_0 \to 180°$, while I_f tends to a finite negative value. Apparently, the electromagnetic forces contribute to the momentum value at the origin.

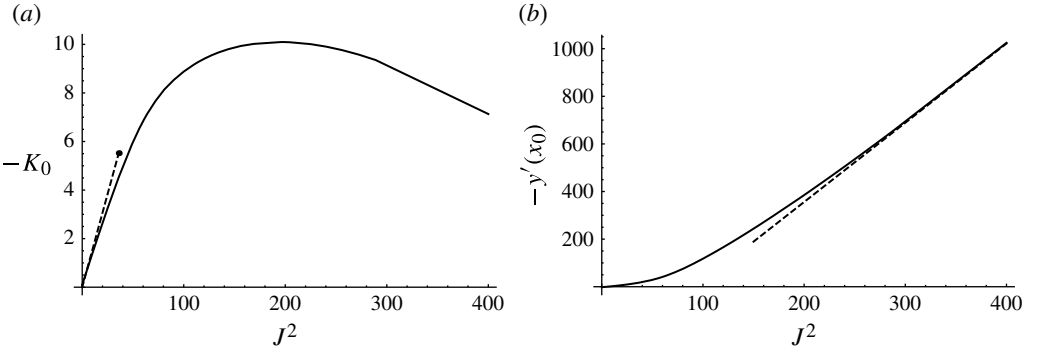


FIGURE 12. Non-swirling jet. Solid lines correspond to the numerical solutions of (3.1) and (7.6) with $y'(1) = -Re = -10$ for $x_0 = -0.95$. (*a*) Graph of K_0 against J^2. Dashed line marks the solution with $x_0 = -1$ which obtains a pole at the point $x = -1$ when $J_\infty \approx 6.0293$ and $Bt = 0$ (see figure 6*a*) then $K_0^\infty = -J_\infty^2(1 - \ln 2)/2 = -5.58$. (*b*) Graph of $y'(x_0)$ against J^2. Dashed line corresponds to a linear asymptote.

7.2. *Slip condition on the wall*

Let us turn to the other issue. We use the simplifications of this chapter ($Bt = 0$) and neglect the no-slip condition on the cone (Sozou & English 1972). In this case, the boundary condition on the wall is $y(x_0) = 0$. Equation (3.3) gives

$$F = -\frac{K_0}{2}(1-x)^2 - \frac{2J^2}{(1-x_0)^2}\left(x^2 + (2\ln 2 - 1)x - \frac{(1+x)^2}{2}\ln(1+x)\right). \qquad (7.6)$$

The coefficient K_0 is the same as used by Sozou & English (1972). It is determined numerically so as to satisfy the condition $y(x_0) = 0$. If $x_0 = -1$ and y has a logarithmic singularity at $x = -1$, then $K_0 = -J^2(1 - \ln 2)/2$ (since $F(-1) = 0$) and the limiting value is $K_0^\infty = -5.58$ (see figures 6*a* and 12*a*), otherwise if $x_0 > -1$ and y is analytic

https://doi.org/10.1017/jfm.2014.103 Published online by Cambridge University Press

in the entire domain, K_0 has no limiting value. Figure 12(*b*) shows that $y'(x_0)$ is finite for $x_0 > -1$ and increases linearly with J^2.

7.3. *Summary*

This section shows that the no-slip condition imposes some unusual features. It is the mechanical momentum at the origin which defines the jet like flow. The solution exists when the value of momentum determines the value of the current. Although for the numerical solutions the velocity is zero on the rigid wall, in the limit of a narrow cone the effect of the no-slip condition vanishes (figure 11*a*). For a thin wire ($\theta_0 \to \pi$) the current value tends to zero and the flow field tends to that corresponding to the Slezkin–Landau–Squire solution. At the same time, the momentum reduces due to electromagnetic forces since $I_f \neq 0$, which formally does not depend on the hydrodynamic parameters according to (7.4). However, we find the solution of the problem and determine $J = J(Re)$, with J tending to zero if $x_0 \to -1$ for all Re. Thus, in the limit of the infinitely thin wire the effect of the magnetic field on the flow is eliminated and the no-slip condition on the wall vanishes.

The analysis of Sozou and English problem (when the slip boundary condition for the radial velocity is applied at the wall) but for the small cone angle shows that the singularity does not occur in the flow domain at all values of the current.

8. Conclusion

The work presents the exact solution of the MHD equations in infinite space. The steady flow is induced by the point source of momentum and point electrode discharging the electric current, which are both located at the end of a thin semi-infinite insulated wire. The solution has a self-similar form when the velocity and magnetic field decrease as the inverse distance from the origin. If the wire is infinitely thin, then the no-slip condition cannot be satisfied. In this case, the radial velocity has a logarithmic singularity on the wire; however, the current magnitude J is not a function of the axial momentum of the jet flow and can be set independently.

With the increase in J, a reverse flow occurs along the wire, which causes the confinement of the current density in a certain point of space. At large J, the solution of the boundary-layer type is derived. It is found that the boundary-layer thickness near the wire scales as $J^{-1/f(Bt)}$ ($0 < f \leqslant 1/2$). For $Bt = 0$ the exact solution exists only at finite values of J which is consistent with the boundary-layer analysis since f tends to zero.

We consider the balance of the forces in the vicinity of the wire so as to explain the reverse flow. It is shown that viscous, pressure and Lorentz forces compensate each other in the leading orders.

A pitchfork bifurcation of the poloidal magnetic field is found, which leads to the rotation of the fluid. A physical mechanism of the bifurcation is demonstrated. According to the bifurcation theory, the solution without rotation is likely to lose stability, while a new solution with rotation is expected to be stable. The generation of rotation eliminates the current confinement effect.

The limit of the problem is considered when a narrow cone tends to the wire while the slip condition is set on the wall of the cone. No singularities in the flow region occur, unlike when the cone appears to be a wire (a line). The radial velocity on the cone increases as J^2 at large J. The no-slip condition on the wall (for finite cone angle) results in the following. The current determines the value of the momentum source. When the cone tends to a wire, the effect of the magnetic field on the flow is

https://doi.org/10.1017/jfm.2014.103 Published online by Cambridge University Press

eliminated and the no-slip condition on the wall vanishes. The solution of the MHD problem approaches the Slezkin–Landau–Squire solution. These findings emphasize the relevance of the present formulation when the flow is determined by the Reynolds number and the current which can be set independently.

Acknowledgements

The authors acknowledge Natalia Mullyadzhanova for the help with the translation and JFM referees for their valuable comments. We also thank Dr Egor Dontsov for reading the manuscript. The work of R.I.M. was supported in part by the Government (Lead Scientists Grant No. 11.G34.31.0046 for K. Hanjalić) and the President of Russian Federation (Lead Scientific Schools Grant No. 5984.2014.8 for D.M. Markovich).

Appendix A. Π_{ij} and Λ_{ij} in the spherical coordinate system

Expressions for the components of the symmetric tensor of the total momentum flux Π_{ij} in the spherical coordinate system

$$\begin{aligned}
\Pi_{rr} &= \rho u_r^2 - 2\rho\nu\frac{\partial u_r}{\partial r} + p - \frac{B_r^2}{2\mu},\\
\Pi_{r\theta} &= \rho u_r u_\theta - \rho\nu\left(\frac{1}{r}\frac{\partial u_r}{\partial \theta} + \frac{\partial u_\theta}{\partial r} - \frac{u_\theta}{r}\right) - \frac{B_r B_\theta}{\mu}, \quad \Pi_{\theta r} = \Pi_{r\theta},\\
\Pi_{r\varphi} &= \rho u_r u_\varphi - \rho\nu\left(\frac{1}{r\sin\theta}\frac{\partial u_r}{\partial \varphi} + \frac{\partial u_\varphi}{\partial r} - \frac{u_\varphi}{r}\right) - \frac{B_r B_\varphi}{\mu}, \quad \Pi_{\varphi r} = \Pi_{r\varphi},\\
\Pi_{\theta\theta} &= \rho u_\theta^2 - 2\rho\nu\left(\frac{1}{r}\frac{\partial u_\theta}{\partial \theta} + \frac{u_r}{r}\right) + p - \frac{B_\theta^2}{2\mu},\\
\Pi_{\theta\varphi} &= \rho u_\theta u_\varphi - \rho\nu\left(\frac{1}{r\sin\theta}\frac{\partial u_\theta}{\partial \varphi} + \frac{1}{r}\frac{\partial u_\varphi}{\partial \theta} - \frac{u_\varphi\cot\theta}{r}\right) - \frac{B_\theta B_\varphi}{\mu}, \quad \Pi_{\varphi\theta} = \Pi_{\theta\varphi},\\
\Pi_{\varphi\varphi} &= \rho u_\varphi^2 - 2\rho\nu\left(\frac{1}{r\sin\theta}\frac{\partial u_\varphi}{\partial \varphi} + \frac{u_r}{r} + \frac{u_\theta\cot\theta}{r}\right) + p - \frac{B_\varphi^2}{2\mu}.
\end{aligned} \tag{A 1}$$

Expressions for the components of the antisymmetric tensor Λ_{ij} in the spherical coordinate system

$$\begin{aligned}
\Lambda_{rr} &= 0, \quad \Lambda_{\theta\theta} = 0, \quad \Lambda_{\varphi\varphi} = 0,\\
\Lambda_{r\theta} &= B_r u_\theta - u_r B_\theta - \lambda\left(\frac{1}{r}\frac{\partial B_r}{\partial \theta} - \frac{\partial B_\theta}{\partial r} - \frac{B_\theta}{r}\right), \quad \Lambda_{\theta r} = -\Lambda_{r\theta},\\
\Lambda_{r\varphi} &= B_r u_\varphi - u_r B_\varphi - \lambda\left(\frac{1}{r\sin\theta}\frac{\partial B_r}{\partial \varphi} - \frac{\partial B_\varphi}{\partial r} - \frac{B_\varphi}{r}\right), \quad \Lambda_{\varphi r} = -\Lambda_{r\varphi},\\
\Lambda_{\theta\varphi} &= B_\theta u_\varphi - u_\theta B_\varphi - \lambda\left(\frac{1}{r\sin\theta}\frac{\partial B_\theta}{\partial \varphi} - \frac{1}{r}\frac{\partial B_\varphi}{\partial \theta} - \frac{B_\varphi\cot\theta}{r}\right), \quad \Lambda_{\varphi\theta} = -\Lambda_{\theta\varphi}
\end{aligned} \tag{A 2}$$

Appendix B. Coefficients of the asymptotic expansions

Expressions for the coefficients of the asymptotic expansions (3.6)–(3.10) in the singular point $x = -1$

$$L_{11} = BtJ^3/8 + Bty_{10}J/2, \tag{B 1}$$

https://doi.org/10.1017/jfm.2014.103 Published online by Cambridge University Press

$$y_{21} = -(4+Bt)J^4/128 + ((2+3Bt)y_{10} - 2)J^2/16 - L_{10}J/4, \tag{B 2}$$
$$y_{22} = (2+Bt)J^4/128 - Bty_{10}J^2/16, \tag{B 3}$$
$$f_{20} = -(4+Bt)J^4/64 + ((2+3Bt)y_{10} - 4)J^2/8 - L_{10}J/2 - (y_{10}^2 - 2y_{10} - 4y_{20} - \phi_{10}^2)/2, \tag{B 4}$$
$$f_{21} = BtJ^4/64 + Bty_{10}J^2/8 - L_{10}J/2, \tag{B 5}$$
$$f_{22} = -BtJ^4/64 - Bty_{10}J^2/8, \tag{B 6}$$
$$L_{20} = Bt(38+17Bt)J^5/1024 - Bt((5+7Bt) - 3)J^3/64 + 3BtL_{10}J^2/32 + Bt(y_{10} - Bty_{10}^2 + 3y_{20})J/4 + Bt(L_{10}y_{10} - \gamma_{10}\phi_{10})/2, \tag{B 7}$$
$$L_{21} = -11Bt(2+Bt)J^5/512 + Bt((3+4Bt)y_{10} - 1)J^3/32 - BtL_{10}J^2/16 + Bt^2y_{10}^2J/4, \tag{B 8}$$
$$L_{22} = 3Bt(1+Bt)J^5/256 + 3Bt^2y_{10}J^3/64, \tag{B 9}$$
$$\gamma_{20} = Bt\phi_{10}J^3/128 - 3\gamma_{10}J^2/32 + Bty_{10}\phi_{10}J/16 + (y_{10}\gamma_{10} - L_{10}\phi_{10})/4, \tag{B 10}$$
$$\gamma_{21} = -Bt\phi_{10}J^3/64 + \gamma_{10}J^2/16 - Bty_{10}\phi_{10}/8, \tag{B 11}$$
$$\phi_{20} = -Bt\phi_{10}J^2/16. \tag{B 12}$$

Apparently, all coefficients are expressed by y_{10}, y_{20}, L_{10}, γ_{10} and ϕ_{10}.

Expressions for the coefficients of the asymptotic expansions (3.11)–(3.15) in the singular point $x = 1$

$$y_2 = -Re/2 - Re^2/4 - f_2/2 + \phi_1^2/4, \tag{B 13}$$
$$L_2 = -BtL_1Re/2 + Bt\gamma_1\phi_1/2, \tag{B 14}$$
$$\gamma_2 = -Re\gamma_1/4 + L_1\phi_1/4. \tag{B 15}$$

The coefficients L_1, γ_1, ϕ_1 and f_2 remain indeterminate.

Appendix C. Balance of the forces in the vicinity of the wire

Expressions for r components have the following form: total pressure force

$$(\nabla p_t)_r = -\frac{\rho v^2}{2r^3}\left(\frac{J^2}{\epsilon} - \frac{BtJ^4}{24}\ln^3\epsilon + \varkappa_2^p\ln^2\epsilon + \varkappa_1^p\ln\epsilon + \varkappa_0^p + o(1)\right),$$
$$\varkappa_i^p = \varkappa_i^b + \varkappa_i^v - 2\varkappa_i^c, \quad i = 0, 1, 2; \tag{C 1}$$

Lorentz force (without magnetic pressure)

$$\frac{1}{\mu}(\boldsymbol{B}\cdot\nabla\boldsymbol{B})_r = -\frac{\rho v^2}{2r^3}\left(\frac{J^2}{\epsilon} + \varkappa_2^b\ln^2\epsilon + \varkappa_1^b\ln\epsilon + \varkappa_0^b + o(1)\right),$$
$$\varkappa_2^b = 2JL_{12}; \quad \varkappa_1^b = 2JL_{11}, \quad \varkappa_0^b = \tfrac{J^2}{2} + 2JL_{10} + 2\phi_{10}^2; \tag{C 2}$$

viscous force

$$\rho\nu(\nabla^2\boldsymbol{u})_r = \frac{\rho v^2}{2r^3}\left(\frac{BtJ^4}{24}\ln^3\epsilon + \varkappa_2^v\ln^2\epsilon + \varkappa_1^v\ln\epsilon + \varkappa_0^v + o(1)\right); \quad \varkappa_2^v = 8y_{22} + 60y_{23},$$
$$\varkappa_1^v = 8y_{21} + 40y_{22} + 96y_{23}, \quad \varkappa_0^v = -2y_{11} + 8y_{20} + 20y_{21} + 32y_{22} + 24y_{23}. \tag{C 3}$$

https://doi.org/10.1017/jfm.2014.103 Published online by Cambridge University Press

The radial component of the inertial force equals

$$F_r = \rho(\boldsymbol{u}\cdot\nabla\boldsymbol{u})_r = -\frac{\rho\nu^2}{r^3}(\varkappa_2^c \ln^2\epsilon + \varkappa_1^c \ln\epsilon + \varkappa_0^c + o(1)), \tag{C 4}$$

$$\varkappa_2^c = \frac{J^4}{16}, \quad \varkappa_1^c = \frac{J^2}{2}\left(\frac{3J^2}{8} + y_{10}\right), \quad \varkappa_0^c = \tfrac{1}{16}(J^4 + 12J^2 y_{10} + 16y_{10}^2).$$

Expressions for θ-components have the following form: total pressure force

$$(\nabla p_t)_\theta = \frac{\rho\nu^2}{r^3}\sqrt{\frac{\epsilon}{8}}\left(\frac{J^2}{\epsilon^2} + \frac{BtJ^4}{8\epsilon}\ln^2\epsilon + \frac{BtJ^2}{\epsilon}(J^2+4y_{10})\ln\epsilon + \frac{J}{4\epsilon}(3J+8L_{10}) + \frac{Bt^2J^6}{256}\ln^4\epsilon + \tau_3^p\ln^3\epsilon + \tau_2^p\ln^2\epsilon + \tau_1^p\ln^1\epsilon + \tau_0^p + o(1)\right),$$

$$\tau_3^p = \frac{BtJ^4}{384}(9BtJ^2 + 24Bty_{10} - 16), \quad \tau_i^p = \tau_i^b + \tau_i^\nu - 2\tau_i^c, \quad i = 0, 1, 2; \tag{C 5}$$

Lorentz force (without magnetic pressure)

$$\frac{1}{\mu}(\boldsymbol{B}\cdot\nabla\boldsymbol{B})_\theta = \frac{\rho\nu^2}{r^3}\sqrt{\frac{\epsilon}{8}}\left(\frac{J^2}{\epsilon^2} + \frac{BtJ^4}{8\epsilon}\ln^2\epsilon + \frac{2JL_{11}}{\epsilon}\ln\epsilon + \frac{2JL_{10}}{\epsilon} - \frac{J^2}{4\epsilon} + \frac{Bt^2J^6}{256}\ln^4\epsilon + 2(L_{11}L_{12}+JL_{23})\ln^3\epsilon + \tau_2^b\ln^2\epsilon + \tau_1^b\ln\epsilon + \tau_0^b + o(1)\right),$$

$$\tau_2^b = L_{11}^2 - \frac{JL_{12}}{2} + 2L_{10}L_{12} + 2JL_{22}, \quad \tau_1^b = 2L_{10}L_{11} - \frac{JL_{11}}{2} + 2JL_{21}, \tag{C 6}$$

$$\tau_0^b = -\frac{9J^2}{32} - \frac{JL_{10}}{2} + L_{10}^2 + 2JL_{20} - \phi_{10}^2; \tag{C 7}$$

viscous force

$$\rho\nu(\nabla^2\boldsymbol{u})_\theta = \frac{\rho\nu^2}{r^3}\sqrt{\frac{\epsilon}{8}}\left(\frac{J^2}{\epsilon} - \frac{BtJ^4}{24}\ln^3\epsilon + \tau_2^\nu\ln^2\epsilon + \tau_1^\nu\ln\epsilon + \tau_0^\nu + o(1)\right),$$

$$\tau_2^\nu = 8y_{22} + 36y_{23}, \quad \tau_1^\nu = 8y_{21} + 24y_{22} + 24y_{23}, \quad \tau_0^\nu = -y_{11} + 8y_{20} + 12y_{21} + 8y_{22}. \tag{C 8}$$

The poloidal component of the inertial force equals

$$F_\theta = \rho(\boldsymbol{u}\cdot\nabla\boldsymbol{u})_\theta = -\frac{\rho\nu^2}{r^3}\sqrt{\frac{\epsilon}{8}}(\tau_2^c\ln^2\epsilon + \tau_1^c\ln\epsilon + \tau_0^c + o(1)), \tag{C 9}$$

$$\tau_2^c = \frac{J^4}{16}, \quad \tau_1^c = \frac{J^2(J^2+4y_{10})}{8}, \quad \tau_0^c = \gamma_{10}^2 - y_{10}^2 - \frac{J^2y_{10}}{2}.$$

We can conclude that the region of the reverse flow occurs in the vicinity of the wire due to the cumulative effect of the viscous, pressure and Lorentz forces. The radial forces eliminate each other in orders ϵ^{-1} and $\ln^3\epsilon$, while the leading order of the inertial force (C 4) has $\ln^2\epsilon$ dependence. At the same time, the five first terms of the poloidal forces compensate for each other and the leading order of the inertial force (C 9) is $\sqrt{\epsilon}\ln^2\epsilon$.

https://doi.org/10.1017/jfm.2014.103 Published online by Cambridge University Press

Appendix D. Coefficients of the asymptotic expansions of the boundary layer equations

Expressions for the coefficients of the asymptotic expansions (5.5) and (5.6) in the singular point $\eta = 0$

$$y_{11} = 1/8, \tag{D 1}$$
$$L_{11} = Bt(1 + 8y_{10})/16, \tag{D 2}$$
$$L_{12} = Bt/32, \tag{D 3}$$
$$y_{21} = (32y_{10} - 64L_{10} - 4 + Bt(48y_{10} - 1))/512, \tag{D 4}$$
$$y_{22} = (2 + Bt(1 - 16y_{10}))/512, \tag{D 5}$$
$$L_{20} = Bt(Bt(17 - 224y_{10} - 1024y_{10}^2) + 2(19 - 80y_{10} + 32L_{10}(3 + 32y_{10}) + 1536y_{20}))/4096, \tag{D 6}$$
$$L_{21} = Bt(96y_{10} - 64L_{10} - 22 + Bt(512y_{10}^2 + 128y_{10} - 11))/2048, \tag{D 7}$$
$$L_{22} = 3Bt(1 + Bt(1 + 8y_{10}))/1024, \tag{D 8}$$
$$L_{23} = Bt^2/1024. \tag{D 9}$$

Expressions for the coefficients of the asymptotic expansions (5.7) and (5.8) in the point $\eta = \infty$ $(\delta = Bt\, y_\infty)$

$$y_1 = -L_1^2/(4y_\infty(2Bt - 1)(\delta^2 - 1)),$$

$$y_2 = \frac{L_1^4(2 + Bt\delta(y_\infty - 6) + Bt(10\delta^2 + 9y_\infty - 4))}{768y_\infty^3(2Bt - 1)^2(\delta - 1)^2(\delta + 1)^4(4 + 2y_\infty(9Bt - 1) + 5\delta y_\infty(4Bt - 1))}, \tag{D 10}$$

$$L_2 = -Bt^2L_1^3(2 + 5\delta)/(24(2Bt - 1)\delta^2(\delta - 1)(\delta + 1)^2), \tag{D 11}$$

$$L_3 = \frac{Bt^4L_1^5(12 + 56\delta + 19\delta^2 - 61\delta^3 + 2Bt(4 + 64\delta + 209\delta^2 + 185\delta^3))}{768(2Bt - 1)^2(\delta - 1)^2\delta^3(\delta + 1)^4(5\delta + 2)(2Bt(2\delta + 1) - \delta)}. \tag{D 12}$$

REFERENCES

ARNOLD, V. I., AFRAJMOVICH, V. S., ILYASHENKO, Y. S. & SHILNIKOV, L. P. 1999 *Bifurcation Theory and Catastrophe Theory*. Springer.

BOJAREVICS, V. 1981 MHD flows due to an electric current point source. Part 1. *Magn. Gidrodin.* **1**, 21–28.

BOJAREVICS, V., FREIBERGS, J., SHILOVA, E. I. & SCHERBININ, E. V. 1989 *Electrically Induced Vortical Flows*. Kluwer.

BOJAREVICS, V., MILLERE, R. & CHAIKOVSKY, A. I. 1981 Investigation of the azimuthal perturbation growth in the flow due to an electric current point source. In *Proc. 10th Riga Conf. on MHD, Riga, Latvia*, Vol. 1, pp. 147–148.

BOJAREVICS, V. & SHCHERBININ, E. V. 1983 Azimuthal rotation in the axisymmetric meridional flow due to an electric-current source. *J. Fluid Mech.* **126**, 413–430.

DAVIDSON, P. A. 2001 *An Introduction to Magnetohydrodynamics*. Cambridge University Press.

DAVIDSON, P. A., KINNEAR, D., LINGWOOD, R. J., SHORT, D. J. & HE, X. 1999 The role of Ekman pumping and the dominance of swirl in confined flows driven by Lorentz forces. *Eur. J. Mech.* B *Fluids* **18**, 693–711.

GOLDSHTIK, M. A. 1960 A paradoxial solution of the Navier–Stokes equations. *Prikl. Mat. Mekh.* **24**, 610–621.

GOLDSHTIK, M. A. 1979 On swirling jets. *Fluid Dyn.* **14** (1), 19–26.

GOLDSHTIK, M. A. & SHTERN, V. N. 1989 The self-similar hydromagnetic dynamo. *Zh. Eksp. Teor. Fiz.* **96**, 1728–1743.

https://doi.org/10.1017/jfm.2014.103 Published online by Cambridge University Press

GRANTS, I., ZHANG, C., ECKERT, S. & GERBETH, G. 2008 Experimental observation of swirl accumulation in a magnetically driven flow. *J. Fluid Mech.* **616**, 135–152.

LANDAU, L. D. 1944 On a new exact solution of the Navier–Stokes equations. *Dokl. Akad. Nauk SSSR* **43**, 299–301.

LANDAU, L. D. & LIFSHITZ, E. M. 1987 *Fluid Mech*. Pergamon Press.

LONG, R. R. 1958 Vortex motion in a viscous fluid. *J. Met.* **15**, 108–112.

LONG, R. R. 1961 A vortex in an infinite viscous fluid. *J. Fluid Mech.* **11**, 611–624.

LUNDQUIST, L. D. 1969 On the hydromagnetic viscous flow generated by a diverging electric current. *Ark. Fys.* **40**, 89–95.

MOREAU, R. 1990 *Magnetohydrodynamics*. Kluwer, Dordrecht.

NARAIN, J. P. & UBEROI, M. S. 1971 On the hydromagnetic viscous flow generated by a diverging electric current. *Phys. Fluids* **14**, 2687–2692.

NARAIN, J. P. & UBEROI, M. S. 1973 Fluid motion caused by conical currents. *Phys. Fluids* **14**, 940–942.

PAO, H. P. & LONG, R. R. 1966 Magnetohydrodynamic jet vortex in a viscous conducting fluid. *Q. J. Mech. Appl. Maths* **19**, 1–26.

PETRUNIN, A. A. & SHTERN, V. N. 1993 Bifurcation of poloidal field in the flow induced by a radial electric current. *Fluid Dyn.* **28** (2), 160–165.

SERRIN, J. 1972 The swirling vortex. *Phil. Trans. R. Soc. Lond.* A **271** (1214), 327–360.

SHCHERBININ, E. V. 1969 On a class of exact solutions in the magnetohydrodynamics. *Magn. Gidrodin.* **4**, 46–58.

SHCHERBININ, E. V. 1973 Jet flows in an electric arc. *Magn. Gidrodin.* **4**, 66–72.

SHERCLIFF, J. A. 1970 Fluid motion due to an electric current source. *J. Fluid Mech.* **40**, 241–250.

SHTERN, V. 2012 *Counterflows: Paradoxical Fluid Mechanics Phenomena*. Cambridge University Press.

SHTERN, V. & BARRERO, A. 1995 Bifurcation of swirl in liquid cones. *J. Fluid Mech.* **300**, 169–205.

SHTERN, V. & HUSSAIN, F. 1998 Instabilities of conical flows causing steady bifurcations. *J. Fluid Mech.* **366**, 33–85.

SHTERN, V. & HUSSAIN, F. 1999 Collapse, symmetry breaking, and hysteresis in swirling flows. *Annu. Rev. Fluid Mech.* **31**, 537–566.

SLEZKIN, M. A. 1934 On a case of integrability of the complete differential equations of a viscous fluid. *Uch. Zap. MGU* **2**, 89–90.

SOZOU, C. 1971 On the fluid motions induced by an electric current source. *J. Fluid Mech.* **46**, 25–32.

SOZOU, C. 1972 Flow motions induced by an electric current jet. *Phys. Fluids* **15**, 272–276.

SOZOU, C. & ENGLISH, H. 1972 Fluid motions induced by an electric current discharge. *Proc. R. Soc. Lond.* A **329**, 71–81.

SOZOU, C., WILKINSON, L. C. & SHTERN, V. N. 1994 On conical swirling flows in an infinite fluid. *J. Fluid Mech.* **276**, 261–271.

SQUIRE, H. B. 1951 The round laminar jet. *Q. J. Mech. Appl. Maths* **4**, 321–329.

SQUIRE, H. B. 1952 Some viscous fluid flow problems. I: jet emerging from a hole in a plane wall. *Phil. Mag.* **43**, 942–945.

TRIBEL, H. 1978 *Interpolation Theory, Function Spaces, Differential Operators*. North Holland.

TSINOBER, A. B. 1973 Axial-symmetric magnetohydrodynamic Stokesian flow in a half-space. *Magn. Gidrodin.* **4**, 17–30.

WU, C.-S. 1961 A class of exact solutions of the magnetohydrodynamic Navier–Stokes equations. *Q. J. Mech. Appl. Maths* **14**, 1–19.

YIH, C.-S., WU, F., GARG, A. K. & LEIBOVICH, S. 1982 Conical vortices: a class of exact solutions of the Navier–Stokes equations. *Phys. Fluids* **25**, 272–276.

https://doi.org/10.1017/jfm.2014.103 Published online by Cambridge University Press